An investigation into the photochemistry of, and the electrochemically induced CO-loss from, [(CO)5MC(OMe)Me](M = Cr or W) using low-temperature matrix isolation, picosecond infrared spectroscopy, cyclic voltammetry, and time-dependent density functional theory

McMahon, S.; Amirjalayer, S.; Buma, W.J.; Halpin, Y.; Long, C.; Rooney, A.D.; Woutersen, S.; Pryce, M.T.

DOI
10.1039/c5dt01568e

Publication date
2015

Document Version
Final published version

Published in
Dalton Transactions

Dalton Transactions

PAPER

View Article Online
View Journal | View Issue

Cite this: *Dalton Trans.*, 2015, **44**, 15424

An investigation into the photochemistry of, and the electrochemically induced CO-loss from, $[(CO)_5MC(OMe)Me]$(M = Cr or W) using low-temperature matrix isolation, picosecond infrared spectroscopy, cyclic voltammetry, and time-dependent density functional theory†

Suzanne McMahon,[a] Saeed Amirjalayer,[b] Wybren J. Buma,[c] Yvonne Halpin,[a] Conor Long,[a] A. Denise Rooney,[d] Sander Woutersen[c] and Mary T. Pryce*[a]

Received 25th April 2015,
Accepted 3rd June 2015

DOI: 10.1039/c5dt01568e

www.rsc.org/dalton

The photophysics and photochemistry of $[(CO)_5MC(OMe)Me]$ (M = Cr or W) were investigated using picosecond time-resolved infrared spectroscopy (M = Cr or W), low-temperature matrix isolation techniques (M = Cr), and time-dependent density functional calculations (M = Cr or W). These studies provide unambiguous evidence for the photochemical formation of a long-lived, 18-electron metallaketene species capable of acting as a synthetically useful intermediate. For the Cr complex, an intermediate metallacyclopropanone singlet excited state was detected on the reaction path to the metallaketene species. This metallacyclopropanone excited state species has a lifetime of less than 100 ps and a characteristic bridging carbonyl band at 1770 cm^{-1}. The tungsten ketene species was also detected but in contrast to the chromium system, this forms directly from a low-lying triplet excited state. The electrochemical release of CO showed a greater efficiency for the chromium complex when compared to the tungsten.

Introduction

Fischer carbene complexes such as $[(CO)_5CrC(OMe)(Me)]$ (**1**), have been extensively studied, because of their ability to act as reagents in organic syntheses.[1–5] A wide range of compounds can be formed using Fischer carbenes including β-lactams, cyclobutanones, β-lactones or amino esters when the carbenes are irradiated in the presence of imines, alkenes, aldehydes or alcohols respectively.[6,7] These reactions are efficient and highly diastereoselective. The terminal carbon of the olefin appears α-to the ketone carbon and the hetero groups adopt a predominantly *anti* disposition in the cyclobutanone product. The ketone functionality originates as a carbonyl ligand on the chromium atom and the reaction mechanism is thought to involve a metallacyclopropanone (**2**) or metallaketene (**3**) intermediate produced in a photoinitiation step.[8] It is important, at the outset, to distinguish between metallacyclopropanones and metallaketenes because they exhibit different spectroscopic properties. In fact, these two structures represent the extreme descriptions of the bonding in this class of complex.[9] For example $(\eta^5\text{-}C_5H_4R)Mn(CO)_2((C_6H_5)_2C{=}C{=}O)$ (R = Me or H) has a metallacyclopropanone structure with a C=C=O angle of 145° and a $\nu_{CC=O}$ absorption at 1787 cm^{-1} in the so-called bridging carbonyl region.[10,11] In *trans*-$Ir(P(i\text{-}Pr)_3)_2Cl$(diphenylketene) however, the ketene ligand coordinates to the Ir atom as a $(\eta^2\text{-}C,O)$ ligand.[12] The C=C=O angle is 136.6(4)° and the $\nu_{CC=O}$ absorption occurs at 1636 cm^{-1} *i.e.* to the low energy side of the bridging carbonyl region. The spectroscopic characterisation of the $(\eta^5\text{-}C_5H_5)Fe(CO)_2(CH_2CO)^+PF_6^-$ salt is consistent with an almost linear ketene unit and importantly this complex exhibits ν_{CO} bands only in the terminal region of the infrared spectrum (1800 to 2100 cm^{-1}).[13] Thus the IR properties of these species are very sensitive to the coordination mode of the ketene. Consequently we believe that it is important to distinguish between these various coordination modes

[a]*School of Chemical Sciences, Dublin City University, Dublin 9, Ireland. E-mail: mary.pryce@dcu.ie; Tel: +353 1 7008005*
[b]*Centre for Nanotechnology (CeNTech) and Institute of Physics, University of Münster, 48149 Münster, Germany*
[c]*University of Amsterdam, Van't Hoff Institute for Molecular Sciences, Science Park 904, 1098 XH, Amsterdam, P.O. Box 94157 1090 GD Amsterdam, The Netherlands*
[d]*Department of Chemistry, Maynooth University, Maynooth, Co. Kildare, Ireland*
†Electronic supplementary information (ESI) available: A listing of calculated coordinates and structural parameters along with calibration details and kinetic analyses and electronic structure details are available. See DOI: 10.1039/c5dt01568e

and the C═C═O angle is an important structural motif in this regard. We classify the coordination mode which exhibits a feature in the bridging CO region and with a C═C═O angle close to 140°, as metallacyclopropanones. Species with near linear C═C═O units (C═C═O angles around 170°) we classify as metallaketenes.[8] These species will exhibit a $\nu_{CC=O}$ feature in the terminal metal carbonyl region.

Previous theoretical studies have suggested that the primary photophysical process following excitation of (**1**) is the formation of a triplet excited state.[14] This, in turn, was reported to yield a triplet metallaketene species which relaxes to the singlet surface by coordination of a molecule of solvent. Given the small spin–orbit coupling of chromium[15] and the proposal that the triplet metallaketene reacts with the singlet solvent molecule,[16] it is important to present additional experimental results to provide a fuller understanding of the photophysical and photochemical processes underpinning this important reaction.

A number of low temperature and time-resolved studies have reported the photochemistry of Fischer carbene complexes such as (**1**), $[(CO)_5WC(OMe)(Ph)]$, $[(CO)_5CrC(OMe)(Ph)]$, $[(CO)_5WC(OMe)(Me)]$ (**4**), or $[(CO)_5CrC(OMe)(biphenyl)]$.[17–21] Photoinduced *anti* to *syn* isomerisation of the carbene ligand and photoinduced CO-loss processes have been reported in these studies. However, no evidence for the formation of a metallacyclopropanone or metallaketene species was obtained. Picosecond time-resolved infrared spectroscopy (psTRIR) is an ideal technique to characterise reactive intermediates and excited states of metal carbonyl complexes, particularly so, because of the high extinctions of the ν_{CO} absorptions. Recently we reported a psTRIR study on the amino Fischer carbene complex $[(CO)_5CrC(NC_4H_8)(Me)]$ and showed that CO loss occurred, during the first 50 ps following excitation at 400 nm *via* an excited state which could be observed spectroscopically.[22] No evidence was obtained for the formation of metallaketene or metallacyclopropanone intermediates. This is, perhaps, not too surprising because many amino Fischer carbene complexes are poor reagents in the synthesis of β-lactams.[23]

Recently, Nguyen *et al.* reported the results of a psTRIR investigation into the photophysics and photochemistry of (**1**) and its tungsten analogue (**4**) in cyclohexane solution using 400 nm wavelength excitation.[24] This study provided fresh insights into the photophysics underpinning the photoinitiated organic transformations using Fischer carbenes, and showed the intermediate formation of excited state species which could be detected by the psTRIR technique. The formation of one short-lived singlet (lifetime 35 ps) and two long-lived triplet (lifetime > 2 ns) species referred to as "Cr-ketenes" was reported. These species have features in the bridging ν_{CO} region, at 1771 and 1791 cm^{-1} for the two triplet species and at 1777 cm^{-1} for the singlet species. As explained above, we prefer to describe these species as metallacyclopropanones (**2**) rather than metallaketenes (**3**) because of their absorption features in the bridging ν_{CO} region. The two triplet species were reported to be the synthetically important intermediates as they are the only photoproducts which were sufficiently long-lived to engage in bimolecular reactions with keteneophiles. This work appeared to support the previously published theoretical study suggesting a role for triplet excited states in these systems.[14] Our results differ fundamentally from those previously published.[14,24] In the experiments reported here, which used lower pulse energies, we do not observe the long-lived triplet excited state species. In addition we observe the formation of an unreported ground state metallaketene which we propose as the intermediate in the reaction of these complexes with keteneophiles. Consequently, it is important to describe our results and the important consequences they have for a fuller understanding of the photophysical and photochemical processes of this important class of molecules.

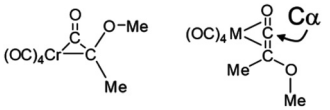

(**2**) (**3**) M = Cr (**6**) M = W

We report the results of a psTRIR investigation of (**1**) and (**4**) and present an alternative route to the reactive metallaketene species to that presented in ref. 24. We also present low-temperature matrix isolation (MI) studies on (**1**) and time-dependent density functional calculations (TDDFT) on (**1**) and (**4**) to support our experimental results. Excited state dynamics along reaction coordinates to either CO-loss or ketene formations are modelled. We present evidence for the formation of the elusive ground-state and long-lived metallaketenes (**3**) and (**6**), which contain no bridging carbonyl ligands. Many years ago Hegedus proposed that these species were the reactive intermediates responsible for cyclobutanone formation.[8] Furthermore our psTRIR studies confirm that for the chromium system, the metallaketene is formed *via* a singlet metallacyclopropanone excited state (**2***, where the asterisk indicates an excited state) which has a lifetime of approximately 30 ps and a bridging ν_{CO} band at 1770 cm^{-1}. For the tungsten analogue (**4**) however, the metallaketene is produced *via* a triplet state which does not contain a bridging CO ligand. As well as being important reagents in organic syntheses, interest is growing in the use of metal carbonyl complexes as reagents for the delivery of CO in a controlled manner.[25] The potential therapeutic applications of CO include vasodilation, anti-inflammatory and anti-proliferative effects. CO releasing molecules (CORMs) have been developed to deliver CO, be it photochemically, thermally or enzymatically induced. Recently we have provided the first evidence that this can be achieved electrochemically.[22] In this paper we show that (**1**) and (**4**) release CO electrochemically.

Experimental

The MI apparatus has been described in detail elsewhere.[26] Infrared spectra were recorded using a Perkin Elmer Spectrum One Fourier-transform spectrophotometer operating at 1 cm^{-1} resolution and acquiring 16 scans per spectrum. The psTRIR

apparatus used UV pump and mid-IR probe pulses generated by a Ti:sapphire laser with a repetition rate of 1 kHz. The UV pump pulse of 400 or 320 nm wavelength and typical pulse energies 0.8 to 1 μJ were generated by SHG. IR probe pulses were generated by difference frequency generation (DFG) of the signal and idler from a BBO-based OPA in $AgGaS_2$. The delay positions were scanned by mechanically adjusting the beam-path of the UV pump using a translation stage. The temporal resolution of 200 fs has been obtained from the FWHM of the pump–probe cross-correlation function recorded in a 1 mm thick layer of Si placed in a sample cell identical to that used for the solutions. All solutions for psTRIR studies were continually circulated through cells fitted with CaF_2 windows (500 μm pathlength). UV/Vis spectra were measured using an Agilent 8453 spectrophotometer, sample solutions were contained in 1 cm quartz cuvettes in spectroscopic grade solvents *e.g.* *n*-heptane. All quantum chemical calculations were performed using the Gaussian 09 program suite (Revision D.01)[27] on either the Stokes or Fionn computers at the Irish Centre for High-End Computing. Fragment contributions to valence orbitals were calculated using the AOMix software.[28,29] Molecular structures were visualized using GaussView.[30]

Complex (**1**) and (**4**) were prepared using a reported method according to Fischer's procedure with minor modifications.[31] A 9.09 mmol sample of the metal hexacarbonyl was dissolved in 25 mL of dry diethyl ether. This solution was then cooled to 0 °C and a 10% molar excess of MeLi in diethyl ether was added drop-wise. The reaction mixture was allowed to reach room temperature and left to stir for 1 hour. The solvent was then removed from the resulting dark brown solution under reduced pressure. The residue was dissolved in 25 mL of water and the pH adjusted to 3–4 using trimethyloxoniumtetrafluoroborate. The product was extracted into dichloromethane dried over anhydrous magnesium sulphate and the solvent removed under reduced pressure resulting in a light brown oil. Washing with cold pentane resulted in a yellow solid ((**1**) 82% yield; (**4**) 66% yield).

At ambient temperatures, (**1**) and (**4**) exist as a mixture of two isomers (*anti* and *syn*) in almost equal amounts. These isomers can be distinguished using IR features in the ν_{C-OMe} region, while the terminal ν_{CO} bands of both isomers are identical within a 1 cm^{-1} error. Other workers have used this isomerisation process to explain the formation of novel features in the ν_{CO} region.[24] Table 1 contains the ν_{CO} band positions for relevant complexes in this study both experimental and simulated by hybrid density functional (B3LYP) methods. The weak feature at 1984 cm^{-1} for (**1**) and 1983 cm^{-1} for (**4**) is a symmetric mode of the four *cis*-carbonyl ligands.

Table 1 The observed and calculated ν_{CO} bands for (**1**), (**3**), (**4**), (**5**) and (**6**)

Complex	Observed FTIR		Observed MI		Observed psTRIR[d]		Calculated[a]	
1	2065	w	2067	w	2058	w	2065	w
	1984	w	1986	w	[b]		1983	w
	1964	m	1961	m	[b]		1960	m
	1948	s	1950		[b]		1951	s
			1945		1940	s	1950	s
3			2040	w	[c]		2050	w
			1988	m	1981	m	1968	m
			1949	s	1945	s	1952	s
			1925	m	1919	m	1936	m
			1911	w			1917	w
4	2073	w			2069	w	2072	w
	1983	w			[b]		1982	w
	1960	m			[b]		1958	m
	1945	s			1935	s	1945	s
							1946	s
5			2043	w	2038	w	2017	w
					[c]		1950	m
			1925	w	[c]		1937	s
			1899	m	1896	m	1899	m
6					2059	w	2050	w
					1983	w	1961	m
					1945	s	1945	vs
					1930	s	1900	m
							1856	vw

[a] See ESI for correction details. [b] Obscured by excited-state absorption. [c] Obscured by parent bleach. [d] Because of calibration issues with the psTRIR detector these band positions are approximately 6 cm^{-1} lower than FTIR values.

Results

Picosecond time resolved infrared studies

The UV/Vis absorption spectra in *n*-heptane are presented in Fig. 1. The spectrum of the tungsten complex (**4**) exhibits a weak shoulder on the low energy side of the lowest energy absorption maximum, and this was assigned to the singlet to triplet transition. This feature is absent in the case of the chromium complex (**1**). This observation is consistent with previous studies which confirmed that optical population of the triplet state in Group 6 metal complexes is only possible for tungsten and not for chromium or molybdenum complexes.[32,33] Two excitation wavelengths were used in these

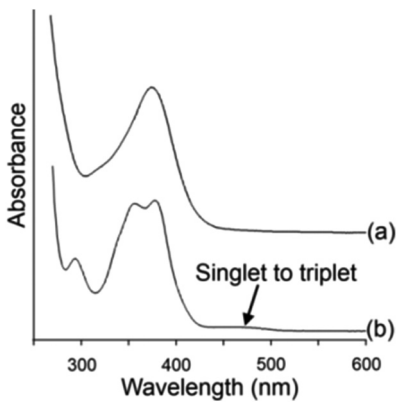

Fig. 1 The UV/Vis spectra of (**1**) (a) and (**4**) (b) recorded in *n*-heptane solution. The singlet to triplet transition is evident as a shoulder in the spectrum of (**4**), this feature is absent in the spectrum of (**1**).

experiments, 400 and 320 nm. The excitation pulse duration was 200 fs with pulse energies of between 0.8 and 1 μJ. Infrared spectral changes were monitored in the 2150–1700 cm^{-1} region covering both the terminal and bridging ν_{CO} regions with a resolution of between 3 and 5 cm^{-1}. All rate constants were measured at 293 K.

psTRIR studies on [(CO)$_5$CrC(OMe)(Me)](1) using 400 nm excitation

The psTRIR difference spectra obtained upon excitation of (**1**) at 400 nm are presented in Fig. 2. Within the excitation pulse the parent bands (2058 and 1940 cm^{-1}) were bleached (negative features in the difference spectrum). A broad feature centred at 1970 cm^{-1} was produced which is assigned to the electronically excited (**1**) *i.e.* (**1***). During the subsequent 10 ps this species decayed and sharper features at 2060, 1986, and 1770 cm^{-1} were produced at the same rate (k_{obs} = 2.4(±0.3)× 10^{11} s^{-1} measured at 2013 $cm^{-1}$for the decay of the 1970 feature and 2.3(±0.2)× 10^{11} s^{-1} measured at 1770 cm^{-1}). This

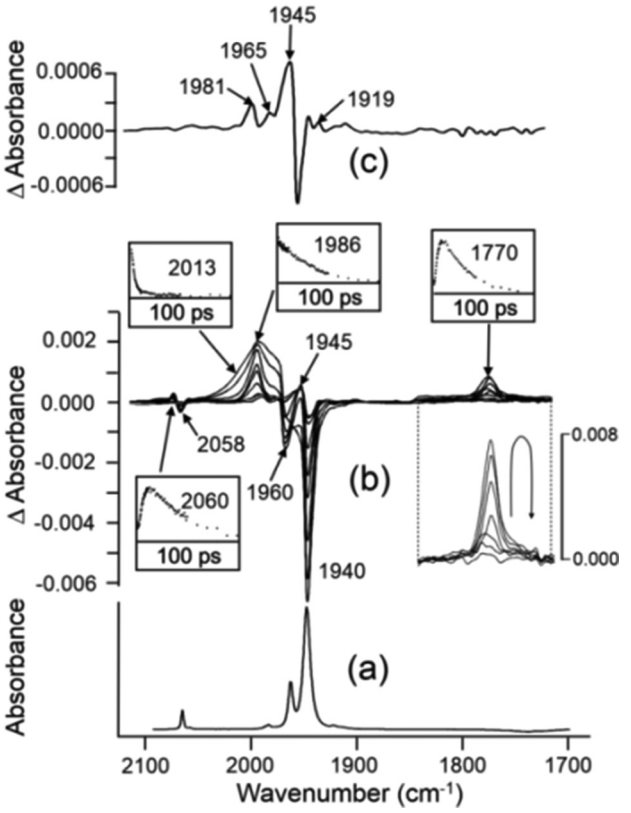

Fig. 2 (a) Is a FTIR spectrum of (**1**) in *n*-heptane solution (b) the psTRIR spectra obtained at 0.4, 2, 6, 30, 50, 100, 120, and 180 ps after 400 nm excitation of (**1**) in *n*-heptane solution showing depletion of the parent bands at 2058, 1960, and 1940 cm^{-1}, the inserts show the time dependence at the indicated wavenumber showing the rapid decay over 10 ps of the broad feature centred at 1970 cm^{-1} (as measured at 2013 cm^{-1}) the growth and decay of the features at 2060 and 1770 cm^{-1} and the decay of the 1986 cm^{-1} feature, and (c) is the expanded final difference spectrum obtained 1500 ps after excitation showing the long-lived features of the metallaketene species at 1981, 1965, 1945, and 1919 cm^{-1}.

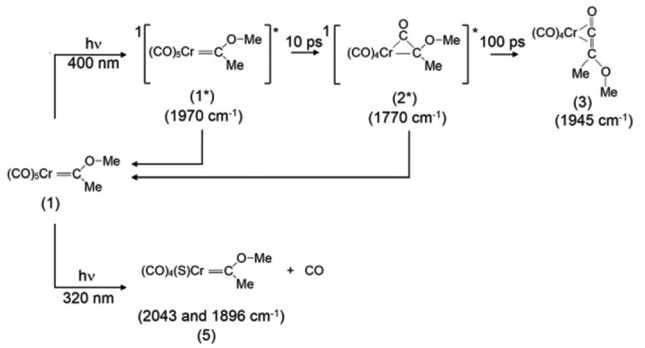

Scheme 1 The photophysical processes of (**1**) leading to the formation of the metallaketene *via* exclusively singlet excited states (diagnostic IR bands in parentheses) and the CO-loss species [(CO)$_4$(S)CrC(OMe)Me] following 320 nm irradiation (S = *n*-heptane).

second species is a metallacyclopropanone excited state (**2***) with a bridging carbonyl ligand absorbing at 1770 cm^{-1}. The metallacyclopropanone excited state in turn decayed (k_{obs} = 2.8(±0.1)× 10^{10} s^{-1}) producing a long-lived (>1.5 ns) metallaketene (**3**), which absorbed at 1981, 1965, 1945, and 1919 cm^{-1} (the latter being very weak) but with no features in the bridging ν_{CO} region (Fig. 2(b)). It is possible that a further weak band is present at approximately 2066 cm^{-1} as the expected residual bleach of the high energy symmetric mode of the parent is absent from spectra obtained at times greater than 1500 ps after excitation (Fig. 2(b)). Fig. 2(a) also contains the time dependent behaviour of selected bands. It should be noted that the parent band at 1940 cm^{-1} recovers with a bi-exponential time dependence (k_1 = 2.0(±0.3)× 10^{11} s^{-1} and k_2 = 3.2(±0.6)× 10^{10} s^{-1}) which means that both the initially produced excited state (**1***) and the metallacyclopropanone excited state (**2***) regenerates the parent (**1**) (Scheme 1). The quantum yield of metallaketene is approximately 0.1 based on the residual depletion of the parent absorbance at 1940 cm^{-1}.

In these experiments, and in contrast to the findings of Nguyen *et al.* who observed the CO-loss product following 400 nm (80 μJ) excitation,[24] 400 nm excitation of (**1**) with 0.8 μJ pulses does not result in appreciable CO-loss. However CO-loss was observed when the pulse energy was increased to 8 μJ *i.e.* the maximum pulse energy possible with our experimental set-up where the resulting damage to the sample solution and deposition of charred products on the cell windows can be briefly tolerated (see ESI for more details†).

psTRIR studies of (1) using 320 nm excitation

The spectroscopic changes observed following 320 nm (0.8 μJ) excitation of (**1**) in *n*-heptane are presented in Fig. 3. Notwithstanding the substantial parent bleach signals, no significant product peaks are observed. The CO-loss product (**5**) at 2043 and 1896 cm^{-1} (k_{obs} = 5.5(±0.9)× 10^{10} s^{-1}) was formed over the subsequent 50 ps and these band positions are consistent with those observed previously for the solvated [(CO)$_4$CrC(C$_4$H$_8$N)-Me] species.[22]

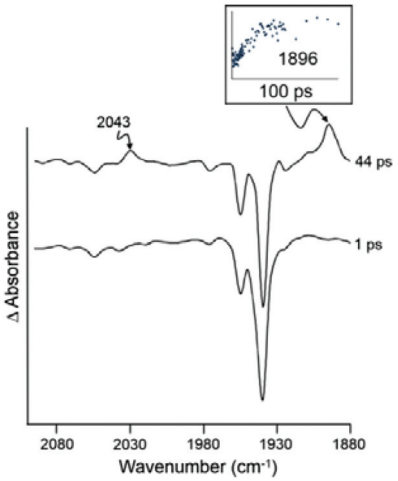

Fig. 3 The infrared spectra obtained 1 and 44 ps after a 320 nm excitation pulse showing the formation of the CO-loss product (**5**) with bands at 2043 and 1896 cm^{-1}.

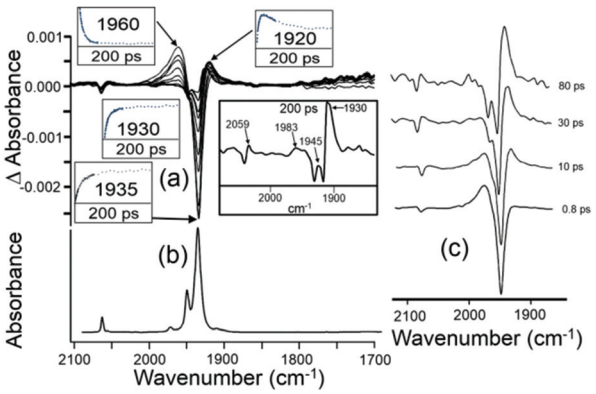

Fig. 4 (a) The psTRIR spectra obtained following 400 nm excitation of (**4**) in *n*-heptane, spectra obtained at 2, 4, 6, 10, 16, 24, 40, 50, 80, 120 and 180 ps after the excitation with the spectrum at 200 ps presented in the boxed inset; the time-dependence of selected bands are also presented in insets, (b) the FTIR spectrum of (**4**) in *n*-heptane and (c) selected spectra at indicated delays after 400 nm excitation showing the initial excited state as a broad feature at 1960 cm^{-1} (the vertical axis is Δ absorbance with various scales).

psTRIR study of (4) using 400 nm excitation

The psTRIR difference spectrum obtained following 400 nm excitation of (**4**) in *n*-heptane is presented in Fig. 4. Within the excitation pulse, the bands of the parent (1935, 1950 cm^{-1} and 2069 cm^{-1}) were depleted and a broad absorption centred at 1965 cm^{-1} was produced (**4*a**). Over the subsequent 20 ps this peak decayed (k = 2.6(±0.9)× 10^{11} s^{-1}) producing a new species with a broad peak at 1920 cm^{-1} and a weak peak at 2051 cm^{-1} (**4*b**) (k = 2.5(±0.1)× 10^{11} s^{-1}). We assign (**4*a**) and (**4*b**) to two triplet excited states with different structures (Scheme 2), the first being directly populated from the ground state in the excitation event (*i.e.* close to the Franck Condon state; see quantum chemical calculations presented below). It should be noted that the UV/vis spectrum of (**4**) exhibits a weak shoulder on the low-energy side of the lowest energy λ_{max} (Fig. 1(b)) which indicates that the direct population of low lying triplet states is possible from the ground state.[15] Over the subsequent 40 ps, the features at 1920 and 2051 cm^{-1} (**4*b**) decay producing absorptions at 1930, 1983 and 2059 cm^{-1} which we assign to the ground state (singlet) metallaketene (**6**) formed by intersystem crossing of the triplet state to the ground-state singlet hypersurface (see inset in Fig. 4 and Scheme 2). Because of the significant spectral overlap of these features with the depleted and recovering parent absorptions it is very difficult to accurately determine peak positions in these experiments. No bands are observed in the bridging carbonyl region which implies that in marked contrast to the chromium system, no metallacyclopropanone excited states are produced in the tungsten system.

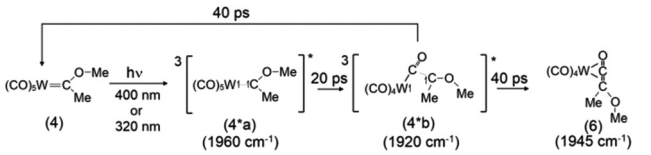

Scheme 2 The photophysical processes following irradiation of (**4**) leading to the metallaketene (**6**) formation *via* triplet excited states, the half arrows indicate the location of large spin density from DFT calculations.

psTRIR study of (4) using 320 nm excitation

The spectral changes observed following excitation of (**4**) using 320 nm light were essentially identical to those observed following excitation at 400 nm described above, with one exception, namely the production of a weak feature at 1886 cm^{-1} assigned to the CO-loss product. The CO-loss product is formed within the excitation pulse (200 fs). Thus the photochemistry of (**4**) is substantially independent of the excitation wavelength, and efficient internal conversion processes occur which predominantly populate the lowest energy triplet state (Scheme 2). No features were observed in the bridging ν_{CO} region following excitation at 320 nm.

Matrix isolation experiments

The MI experiments were performed at 20 K in either pure CH_4 or mixed CH_4 (95%) CO (5%) matrixes. Three excitation regimes were used in these experiments, broad-band irradiation with wavelengths longer than 470 nm, and two monochromatic excitation wavelengths 395 nm or 355 nm. These were chosen to investigate the wavelength dependent nature of the photochemistry of (**1**). It should be noted that 470 nm represents the onset wavelength for the lowest energy absorption of (**1**) and is therefore likely to populate only the lowest accessible singlet excited state. The other two excitation wavelengths span the lowest energy maximum absorbance of (**1**) (Fig. 1). The matrix was subjected to irradiation initially with λ_{exc} > 470 nm followed by irradiation with 395 nm and lastly with 355 nm light.

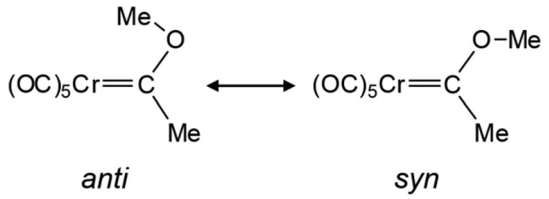

Scheme 3 Representations of the structures of the *anti*- and *syn*-isomers of (**1**).

The infrared spectrum of a freshly deposited sample of (**1**) in either a pure CH_4 matrix or the mixed CH_4/CO matrix at 20 K showed bands in the terminal metal carbonyl region (ν_{CO}) at 2067(w), 1986(w), 1961(s), 1950(shoulder) and 1945(s) cm^{-1}. A weak feature at 1255 cm^{-1} was also observed corresponding to the $C_{carbene}$–OMe stretching vibration. This band is sensitive to the isomeric changes to the carbene ligand while the terminal ν_{CO} bands are not. DFT calculations (described later) indicated that the *anti*-isomer of the (**1**) is slightly more stable than the *syn*-isomer (Scheme 3), and we have therefore assigned these features to the *anti*-isomer which should predominate at 20 K.

Pure CH_4 matrix studies

A freshly deposited matrix of (**1**) was irradiated for 18 hours with λ_{exc} > 470 nm. No changes were observed in the ν_{CO} region of the spectrum following this irradiation. However, the band at 1255 cm^{-1} moved to 1247 cm^{-1} (Fig. S1 in ESI†) indicating *anti*- to *syn*- isomerisation at the carbene ligand. This observation is consistent with earlier studies which also observed an *anti* to *syn* isomerisation of alkoxycarbenes upon photolysis.[18,19] This confirms that the isomerisation is promoted following excitation into the lowest accessible excited state. The failure to observe any significant changes to the terminal ν_{CO} bands following the photoinduced *anti*- to *syn*-isomerisation confirms that both isomers have identical (within experimental error) spectra in this region.

Subsequent irradiation of this matrix using λ_{exc} = 355 nm, resulted in a decrease in the intensity of the ν_{CO} bands of (**1**) and the formation of new ν_{CO} bands at 2043, 1988, 1949 (obscured by parent bleach) 1911, and 1899 cm^{-1} plus the characteristic absorption of "free" CO at 2140 cm^{-1} (Fig. 5(a)). These new bands are assigned to two species, the expected CO-loss species [$(CO)_4$CrC(OMe)(Me)] (**5**) (2043 and 1899 cm^{-1}) and the ketene species (**3**) (2040, 1988, 1949 1925 and 1911 cm^{-1}). These assignments are based on the results presented in this section but also those obtained in psTRIR studies and the DFT calculations described later.

Mixed CH_4/CO matrix studies

A sample of (**1**) was deposited in a mixed matrix consisting of 95% CH_4 and 5% CO. The presence of CO in the matrix was intended to suppress the CO-loss process and allow better observation of other products. Under these conditions, irradiation using 395 nm light produced product bands at

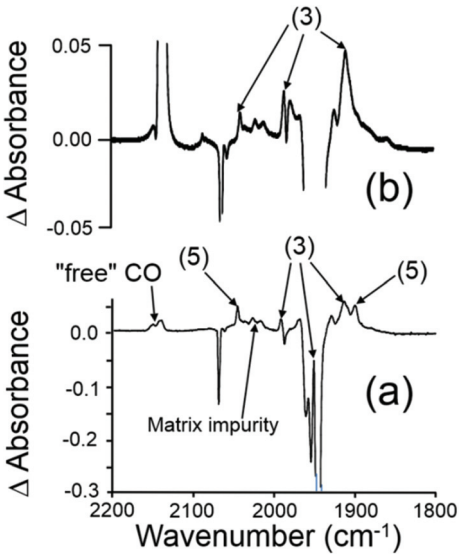

Fig. 5 (a) A difference infrared spectrum obtained following irradiation of (**1**) at 355 nm in a CH_4 matrix at 20 K showing the formation of (**3**) and (**5**) and uncoordinated "free" CO in the matrix and (b) the difference spectrum obtained following irradiation with 395 nm light in a CH_4/CO matrix (95 : 5) showing primarily the formation of (**3**).

2043, 1990, 1949, 1925 and 1911 cm^{-1} (Fig. 5(b)). These bands are assigned to the metallaketene species (**3**). No bridging ν_{CO} bands were observed in these experiments.

Electrochemical CO-loss from [$(CO)_5$CrC(OMe)Me] (**1**) and [$(CO)_5$WC(OMe)Me] (**4**)

Electrochemical analysis of (**1**) and (**4**) were performed in acetonitrile solution using 0.1 M tetrabutylammonium hexafluorophosphate ($TBAPF_6$) as the electrolyte. Cyclic voltammetry reveals a quasi-reversible first oxidation state for (**1**) (E_{pa} = +0.45 V *vs.* Fc/Fc^+) and an irreversible first oxidation for (**4**) (E_{pa} = +0.68 V *vs.* Fc/Fc^+) using a scan rate of 0.1 V s^{-1}. These redox processes are in agreement with those previously reported for these compounds and are assigned to the $Cr^{1/0}$/$W^{1/0}$ redox couple.[34–36] Electrochemically induced CO-loss was measured in acetonitrile at a concentration of 1 mM. Continuous bulk electrolysis was applied at a voltage just greater than the first oxidation potential of the complex, +0.57 and +0.88 for (**1**) and (**4**) respectively (see ESI for more details†). (**1**) liberated 5.28 × 10^{-5} moles of CO after 5478 seconds which equates to ~1 molecule of CO per molecule of complex. Under the same conditions complex (**4**) generated a significantly lower amount of CO (5.92 × 10^{-7} moles).

Quantum chemical calculations

The structures of the *syn*- or *anti*-isomers of (**1**) and (**4**) were optimised to tight convergence at the B3LYP/TZVP level for (**1**) or B3LYP/Def2TZVP level for (**4**)[37–43] Selected bond lengths obtained from these calculations are compared with those obtained from single crystal X-ray diffraction methods in Table S1.† Details of the calculations to derive appropriate cor-

rection factors for the simulated infrared spectral bands for both *syn* and *anti* isomers of (**1**) are also presented in the ESI.†

The photoinduced *syn* to *anti* isomerisation of (1)

The optimised structure of the *syn*-(**1**) was used as a starting point for calculations of the *syn* to *anti* isomerisation of (**1**). The dihedral angle formed by the methyl carbon, the carbene carbon, the methoxy oxygen, and the methoxy carbon was varied between 0° and 180° in steps of 10°. All other structural parameters were optimised in the ground state at each step in these calculations. TDDFT/B3LYP/TZVP[44–46] calculations were performed at each point along this reaction coordinate yielding the vertical excitation energies of the four lowest energy singlet excited states. This plot is presented in the ESI.† We have neglected the triplet excited states as the spin–orbit coupling parameter for chromium(0) is small and direct population of triplet excited states is consequently unlikely under the conditions used in our experiments.[15,32] These data indicate that the *anti*-isomer is only marginally more stable (7 kJ mol^{-1}) than the *syn*-isomer in the ground state and that the two isomers are separated by a thermal barrier of approximately 60 kJ mol^{-1}. Variable temperature ^{1}H NMR studies estimated this barrier as 57 kJ mol^{-1} in dichloromethane solution (see ESI for details†).[47] According to these calculations the predominant isomer in a freshly deposited low temperature matrix (20 K) should be the *anti*-isomer while both isomers will exist in almost equal amounts at room temperature. Examination of the behaviour of the lowest energy singlet excited state (S_1, predominantly a metal carbonyl-to-carbene charge-transfer state) along this reaction coordinate indicates that the *syn*-isomer is slightly more stable than the *anti*-isomer and that the *anti*-*syn* barrier is very small (9 kJ mol^{-1}). Thus population of this excited state, by absorption of a photon with a wavelength of 410 nm, will induce an *anti* to *syn* isomerisation as observed in the low-temperature matrix isolation experiments.

Modelling the metallaketene (3) formation from (1)

The ketene or photocarbonylation of the *syn*-isomer of (**1**) was modeled at the B3LYP/TZVP level. TDDFT methods cannot provide accurate quantitative descriptions of excited state parameters and as a consequence no solvent corrections were applied to these calculations,[48–50] however the approach used here has proved extremely useful in developing a qualitative model for excited state dynamics for large organometallic systems which were then used to explain experimental results.[22,51–59] The reaction coordinate chosen for this study involved reducing the distance between the carbon of one of the *cis* carbonyl ligands (C_α) and the carbene carbon (C_β) (*i.e.* the vector indicated by the dashed line in Fig. 6(a)).

This C_α to C_β distance was reduced from 2.778 to 1.278 Å in steps of 0.1 Å. All other structural parameters were optimised in the ground-state at each step. TDDFT calculations yielded the energy of the four lowest energy singlet excited states at each point along this reaction coordinate. Again only singlet states were considered for the reason outlined above. The resulting plots are presented in Fig. 7(a). These calculations

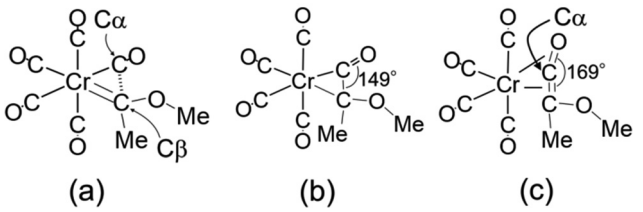

Fig. 6 (a) A representation of the structure of *syn*-(**1**) indicating C_α and C_β and the chosen reaction coordinate to ketene formation as indicated by the dashed line,. (b) the metallacyclopropanone excited state species (**2***) with its bridging carbonyl ligand, and (c) the "bent" metallaketene ground state (**3**).

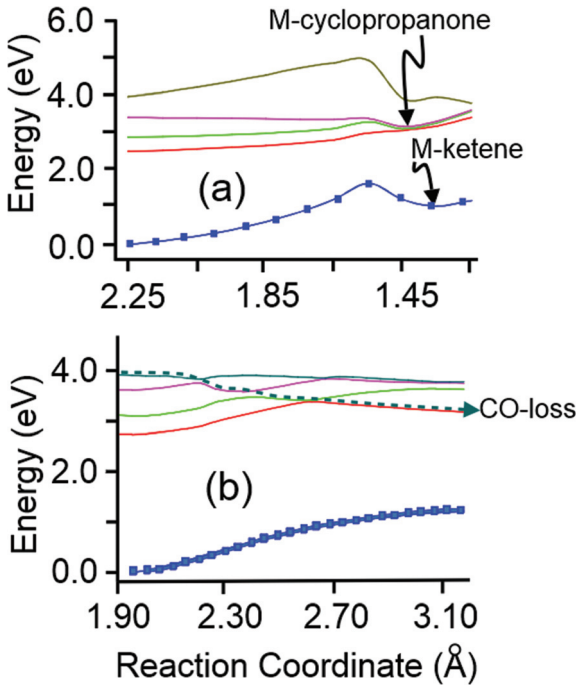

Fig. 7 The adiabatic plots of the ground state and four lowest energy singlet excited states (S_1 to S_4) of *syn*-(**1**) along the reaction coordinates (a) to ketene formation *via* a metallacyclopropanone excited state and (b) to *cis*-CO loss along an unbound state indicated by the dashed curve (see text for further details of the reaction coordinates used; individual data points are indicated on the ground state profile but omitted from the excited state profiles for clarity).

indicate that the metallaketene species (**3**) (Fig. 6(c)) lies along this reaction coordinate at a C_α to C_β distance of 1.347 Å (Cr–C_α 2.056 Å). The ketene fragment is bent with a C_β–C_α–O angle of 169° (optimised coordinates and structural parameters are provided in the ESI†). The infrared spectrum of the ketene species was simulated and the frequency corrected (see ESI†) ν_{CO} bands are predicted at 2050 (w), 1968 (m), 1952 (s) 1936 (m), and 1917 (m) cm^{-1}. These calculations confirm that all the ν_{CO} bands of the metallaketene (**3**) appear in the terminal ν_{CO} region. The calculated Mulliken charge on the chromium atom in the ketene species is only less than that in the carbene

species (−0.764 compared to −1.092 see ESI for a description of the molecular orbital†).

Both the S_2 and S_3 states (predominantly metal carbonyl-to-carbene charge-transfer states) will accelerate the nuclei towards this ketene species. This would require the absorption of a photon with wavelengths between 413 and 345 nm. In the case of each excited state, a small thermal barrier (38 kJ mol^{-1} in the case of S_2 and 4 kJ mol^{-1} for S_3) must be overcome to reach a shallow potential well at a C_α to C_β distance of 1.477 Å. This species is a metallacyclopropanone (**2***) (Fig. 6(b)) and is the excited state precursor to the ground-state metallaketene (**3**). The infrared spectrum of (**2***) will be quite distinct from that of (**3**). This explains the transient appearance of a bridging carbonyl band in the psTRIR studies, as the metallacyclopropanone excited state develops and decays either to the ground-state metallaketene or regenerates the parent carbene complex. Attempts to locate a ketene species starting with the *anti*-isomer of (**1**) failed suggesting that only the *syn*-isomer is implicated in the ketene formation.

The photoinduced CO-loss process from [(CO)$_5$CrC(OMe)Me] (1)

Lengthening of a *cis*-Cr–CO bond length from 1.918 Å to 3.168 Å in steps of 0.05 Å was chosen as a suitable reaction coordinate to model the photoinduced CO-loss process. Structural optimisations on the ground state were undertaken at each step. Based on these structures TDDFT calculations were performed to obtain the vertical excitation energies of the four lowest energy singlet excited states (TDDFT/B3LYP/TZVP). Again only singlet excited states were considered in these calculations. The results are presented in Fig. 7(b). It is clear from this plot that the three lowest energy singlet excited states (S_1, S_2, and S_3) are bound with respect to CO-loss and an additional thermal barrier must be overcome to liberate the *cis*-CO from the metal's coordination sphere in these states. Population of S_3, requiring the absorption of a 340 nm photon, should result in an arrested CO-loss while direct population of S_4, a predominantly metal-to-carbonyl charge-transfer state (317 nm photon), will result in ultrafast CO-loss along the accelerating potential energy profile represented by the dashed curve in Fig. 7(b). The shape of this profile is the result of crossing with a metal-centred state (such as S_{10}) whose energy drops precipitately as the Cr–CO bond length increases in a behaviour similar to that observed in the photo-dissociation of CO from $Cr(CO)_6$.[60–64]

Modelling the metallaketene formation from [(CO)$_5$WC(OMe)Me] (4)

The time-resolved studies on (**1**) and (**4**) confirmed that the photophysical processes of the two systems are quite distinct. It is possible to directly populate triplet states from the singlet ground-state for the tungsten system because of the larger spin orbit coupling for tungsten.[15] The behaviour of the lowest energy triplet state along the reaction coordinate to ketene formation was calculated. The chosen reaction coordinate was similar to the one used for the chromium system and involves reducing the distance between the carbene carbon and a *cis*-carbonyl carbon. A relaxed potential energy scan (B3LYP/Def2TZVP) for the ground-state along this reaction coordinate shows the substantial energy barrier to metallaketene formation (206 kJ mol^{-1}). A similar relaxed potential energy scan was then undertaken for the lowest energy triplet state (UB3LYP/Def2TZVP) presented as the red curve in Fig. 8. The triplet energy profile exhibits a small barrier (22 kJ mol^{-1}) along this reaction coordinate leading to a shallow minimum at a carbene carbon to *cis*-carbonyl carbon distance of 1.91 Å. The singlet and triplet curves meet at a distance of 1.612 Å which corresponds to the transition state of the metallaketene formation on the singlet surface. At this point the metal carbene bond has broken but the inserting metal to carbonyl bond remains intact. This is a branching point on the triplet profile, either to return to the carbene ground-state or proceed to the metallaketene ground-state (indicated by dashed arrows in Fig. 8), both processes involving intersystem crossing to the singlet surface.

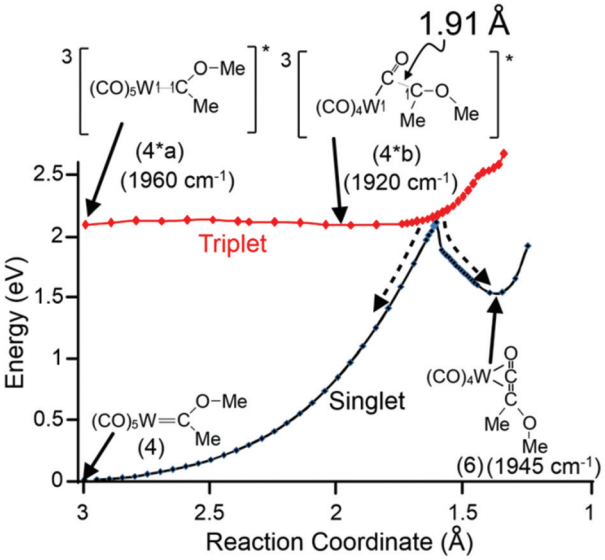

Fig. 8 The behaviour of the ground-state (black, B3LYP/def2-TZVP) and lowest energy triplet state (red, UB3LYP/Def2-TZVP) along the reaction coordinate towards the metallaketene showing the local minimum in the shallow potential energy well at 1.91 Å on the triplet surface and the branching space at the point of degeneracy. Data points are indicated by dots on the profiles and diagnostic IR bands are in parentheses, half arrows indicate the locations of highest spin density for the triplet species.

Discussion

The principal focus of this work is to investigate the photophysical and photochemical processes which underpin the use of group 6 metal carbene complexes as reagents in organic syntheses. We agree with the Nguyen *et al.* assignment of the short lived feature absorbing at 1777 cm^{-1} as a singlet excited state but believe that this is a metallacyclopropanone rather

than a metallaketene species.[24] The evidence we present however, strongly suggests that this species reacts to form a long-lived ground-state metallaketene which we observe both in the psTRIR and MI experiments. In addition we do not observe the triplet species reported by Nguyen *et al.* Consequently an alternative explanation to that proposed by Nguyen *et al.* is that only singlet excited states are involved in the photophysics of (**1**).

It should be noted that in our psTRIR study, typical pulse energies were in the 0.8 to 1 μJ range (with one exception where 8 μJ pulses were used) with a duration of 200 fs. Nguyen *et al.* used pulse energies of 80 μJ and a pulse duration of 1 ps. The proposal that the photophysics of (**1**) remains on the singlet hypersurface is supported by TDDFT calculations. The nature and reactivity of the four lowest energy singlet excited states of (**1**) were calculated, and correlated with the results of our low-temperature MI and psTRIR experiments. The lowest three excited states have significant metal to carbene charge-transfer character but only one, S_3, can be efficiently populated from the ground state. The other two (S_1 and S_2) are the result of symmetry forbidden transitions. The S_4 state has considerable metal-based character and is responsible for the CO-loss process which is not implicated in the useful synthetic pathways to ketene derived products.

Quantum chemical modelling indicates that only the *syn*-isomer can form the reactive metallaketene intermediate which is accessed mainly *via* S_3 (TDDFT calculated vertical excitation energy is 342 nm). The symmetry allowed transition to S_3 is the major contributor to the lowest energy absorption maximum for this complex at 378 nm (Fig. 1). This excited state exists in a shallow potential well (Fig. 7(a)) that can be probed with infrared spectroscopy and detected as the broad absorption centred at 1970 cm^{-1}. This state either relaxes to the ground state or alternatively surmounts a small thermal barrier (4 kJ mol^{-1}) to produce a metallacyclopropanone excited state, which is the precursor to the reactive metallaketene ground state (marked M-cyclopropanone in Fig. 7(a)). It is interesting to note that Hegedus proposed the intermediate formation of this metallacyclopropanone leading to the metallaketene in his seminal work of 1988.[8] It should be pointed out again, that the infrared characteristics of the metallacyclopropanone excited state with a peak in the bridging ν_{CO} region (1770 cm^{-1}) is significantly different to the infrared spectrum of the metallaketene which exhibits ν_{CO} bands only in the terminal M-CO region between 1800 and 2100 cm^{-1}. These structures are represented in Fig. 6.

In contrast to the previous study,[24] we observed no significant CO-loss following 400 nm excitation. Presumably the CO-loss process requires a greater photon flux at 400 nm which may point to sequential multiphoton absorption as observed in our experiment using 8 μJ pulses. TDDFT calculations indicate that the S_4 excited state (316 nm excitation) of (**1**) presents an accelerating profile towards CO-loss (Fig. 7(b)). Surprisingly, in our psTRIR experiments using 320 nm light, no significant absorptions of excited-state species were observed and yet the CO-loss product was formed over approximately 50 ps. This indicates that the CO-loss reaction occurs *via* an unbound or a series of unbound excited states which cannot be probed using infrared spectroscopy (because the vibrational levels are not quantised). This behaviour has been observed in other metal carbonyl systems.[56,61,65]

It is clear from the psTRIR experiments that the photophysics of the tungsten complex (**4**) is significantly different to that of the chromium complex (**1**). Nguyen *et al.* explained the spectroscopic changes by the *anti* to *syn* isomerisation of the carbene ligand,[24] but the results of our study are more consistent with assigning this species as a metallaketene. The metallaketene (**6**) is produced without the intermediate formation of a metallacyclopropanone excited state. Our calculations show that the lowest energy triplet excited state crosses the ground-state along the reaction coordinate to the metallaketene formation (Fig. 8). Consequently we propose that in this case the lowest energy triplet state is responsible for the observed photochemistry.

The experimental data presented here which are supported by quantum chemical calculations show that both the chromium (**1**) and tungsten (**4**) systems form the appropriate metallaketene following suitable irradiation. The lack of photochemical activity of (**4**) towards keteneophiles can be explained as follows. The initial step in the reaction of the metallaketene involves nucleophilic attack at the central ketene carbon (C_α in Fig. 6(c)).[8] Obviously the greater the partial positive charge on the ketene C_α atom the more effective will be the reaction with nucleophilic keteneophiles. The calculated charges on the ketene atoms in (**1**) and (**4**) were obtained from Natural Population Analysis methods along with those of the non-metallated ketene and also the $[(CO)_5MoC(OMe)Me]$ complex. All of these calculations were at the B3LYP/Def2TZVP level using the Polarizable Continuum Model (PCM) to include solvent effects (solvent = heptane). These data are presented in Table 2. The C_α partial charge is +0.621 in the chromium complex is similar to the non-metallated ketene (+0.636) and substantially larger than for either the tungsten complex (+0.480) or the molybdenum (+0.562). These results indicate that in the chromium complex (**3**) the central ketene carbon will act as a good electrophile while in the tungsten or molybdenum complexes (**6**) will be less effective in this regard.[66] This explains the marked difference in reactivity of the group 6 metallaketenes.

Table 2 The charges on the metal (M = Cr, Mo, or W) and the three atoms of the ketene unit using natural population analysis (Fig. 6 for label details) obtained at the B3LYP/Def2TZVP level using a PCM solvent correction (heptane)

		M		
	Ketene	Cr	Mo	W
O	−0.446	−0.380	−0.416	−0.437
C_α	0.636	0.621	0.562	0.480
C	−0.024	0.212	0.187	0.2165
M	—	−1.977	−1.304	−0.986

We have extended our earlier studies to investigate the suitability of both (**1**) and (**4**) as CO releasing molecules under electrochemical conditions. There is a notable difference in the efficiency of CO-loss for (**1**) and (**4**), the chromium complex is the more efficient CO source. Over the timeframe of the experiments, the concentration of CO in the headspace indicates the loss of only one CO molecule per molecule of the complex. These experiments indicate that both (**1**) and the amino analogue [$(CO)_5CrC(C_4H_8N)Me$] release similar quantities of CO.[22]

Conclusions

This work confirms the intermediate role of metallaketene species in the synthetic mechanisms using Fischer carbenes to produce β-lactams and other organic products as first proposed by Hegedus and co-workers in 1988.[8] In contrast to previous experiments which indicated triplet states in the case of the chromium complex, we do not observe any evidence for the formation of triplet states although they may be formed in very low yields.[24] Triplet as well as singlet states have been implicated in the photochemistry of a related imine carbene complex,[67] but our psTRIR experiments indicated that the metallaketene species (**3**) is formed predominantly *via* a singlet excited state. The lowest energy triplet state is implicated in the photochemistry of the tungsten complex however. This is consistent with the larger spin–orbit-coupling for tungsten compared to chromium which facilitates the direct population of triplet states following photolysis. The partial charges on the ketene atoms explain why the chromium metallaketenes are better organic reagents than the tungsten.

Acknowledgements

The authors wish to acknowledge the DJEI/DES/SFI/HEA Irish Centre for High-End Computing (ICHEC) for the provision of computational facilities and support. The authors thank the Amsterdam Laboratory under EU access-LLAMS-1961. We would also like to thank the Irish Research Council RS/2012/341 (SM), and a SFI-13/TIDA/E2763 grant for support (YH and MTP). The authors thank Professor J.M. Kelly for many helpful discussions.

References

1 L. S. Hegedus, *Acc. Chem. Res.*, 1995, **28**, 299–305.
2 K. H. Dotz, *Angew. Chem., Int. Ed. Engl.*, 1984, **23**, 587–608.
3 L. S. Hegedus, M. A. McGuire, L. M. Schultze, C. Yijun and O. P. Anderson, *J. Am. Chem. Soc.*, 1984, **106**, 2680–2687.
4 C. A. Merlic, D. Q. Xu and S. I. Khan, *Organometallics*, 1992, **11**, 412–418.
5 L. S. Hegedus, *Pure Appl. Chem.*, 1990, **62**, 691–698.
6 L. S. Hegedus, *Metal Carbenes in Organic Synthesis*, 2004, **13**, 157–201.
7 M. A. Sierra and L. S. Hegedus, *J. Am. Chem. Soc.*, 1989, **111**, 2335–2336.
8 L. S. Hegedus, G. Deweck and S. D'Andrea, *J. Am. Chem. Soc.*, 1988, **110**, 2122–2126.
9 G. L. Geoffroy, *Adv. Organomet. Chem.*, 1988, **28**, 1–83.
10 W. A. Herrmann, *Angew. Chem., Int. Ed. Engl.*, 1974, **13**, 335–336.
11 A. D. Redhouse and W. A. Herrmann, *Angew. Chem., Int. Ed. Engl.*, 1976, **15**, 615–616.
12 D. B. Grotjahn, L. S. B. Collins, M. Wolpert, G. A. Bikzhanova, H. C. Lo, D. Combs and J. L. Hubbard, *J. Am. Chem. Soc.*, 2001, **123**, 8260–8270.
13 T. W. Bodnar and A. R. Cutler, *J. Am. Chem. Soc.*, 1983, **105**, 5926–5928.
14 I. Fernandez, M. A. Sierra, M. Gomez-Gallego, M. J. Mancheno and F. P. Cossio, *Chem. – Eur. J.*, 2005, **11**, 5988–5996.
15 G. M. Cole and B. B. Garrett, *Inorg. Chem.*, 1970, **9**, 1898–1902.
16 E. Wigner, *Nachr. Ges. Wiss. Gottingen (Math. Phys. Kl.)*, 1927, 375–381.
17 S. E. J. Bell, K. C. Gordon and J. J. McGarvey, *J. Am. Chem. Soc.*, 1988, **110**, 3107–3112.
18 P. C. Servaas, D. J. Stufkens and A. Oskam, *J. Organomet. Chem.*, 1990, **390**, 61–71.
19 M. L. Gallagher, J. B. Greene and A. D. Rooney, *Organometallics*, 1997, **16**, 5260–5268.
20 K. O. Doyle, M. L. Gallagher, M. T. Pryce and A. D. Rooney, *J. Organomet. Chem.*, 2001, **617**, 269–279.
21 A. D. Rooney, J. J. McGarvey and K. C. Gordon, *Organometallics*, 1995, **14**, 107–113.
22 S. McMahon, J. Rochford, Y. Halpin, J. C. Manton, E. C. Harvey, G. M. Greetham, I. P. Clark, A. D. Rooney, C. Long and M. T. Pryce, *Phys. Chem. Chem. Phys.*, 2014, **16**, 21230–21233.
23 A. Hafner, L. S. Hegedus, G. Deweck, B. Hawkins and K. H. Dotz, *J. Am. Chem. Soc.*, 1988, **110**, 8413–8421.
24 S. C. Nguyen, J. P. Lomont, M. C. Zoerb, P. V. Pham, J. F. Cahoon and C. B. Harris, *Organometallics*, 2014, **33**, 6149–6153.
25 W.-Q. Zhang, A. C. Whitwood, I. J. S. Fairlamb and J. M. Lynam, *Inorg. Chem.*, 2010, **49**, 8941–8952.
26 C. Long, K. Maher and M. T. Pryce, *J. Organomet. Chem.*, 2006, **691**, 3298–3304.
27 J. Frisch, G. W. Trucks, H. B. Schlegel, G. E. Scuseria, M. A. Robb, J. R. Cheeseman, G. Scalmani, V. Barone, B. Mennucci, G. A. Petersson, H. Nakatsuji, M. Caricato, X. Li, H. P. Hratchian, A. F. Izmaylov, J. Bloino, G. Zheng, J. L. Sonnenberg, M. Hada, M. Ehara, K. Toyota, R. Fukuda, J. Hasegawa, M. Ishida, T. Nakajima, Y. Honda, O. Kitao, H. Nakai, T. Vreven, J. A. Montgomery, J. E. Peralta, F. Ogliaro, M. Bearpark, J. J. Heyd, E. Brothers, K. N. Kudin, V. N. Staroverov, R. Kobayashi, J. Normand, K. Raghavachari, A. Rendell, J. C. Burant, S. S. Iyengar, J. Tomasi, M. Cossi, N. Rega, J. M. Millam, M. Klene, J. E. Knox, J. B. Cross, V. Bakken, C. Adamo, J. Jaramillo,

R. Gomperts, R. E. Stratmann, O. Yazyev, A. J. Austin, R. Cammi, C. Pomelli, J. W. Ochterski, R. L. Martin, K. Morokuma, V. G. Zakrzewski, G. A. Voth, P. Salvador, J. J. Dannenberg, S. Dapprich, A. P. Daniels, O. Farkas, J. B. Foresman, J. V. Ortiz, J. Cioslowski and D. J. Fox, Gaussian, Inc., Wallingford CT, Editon edn, 2009.

28 S. I. Gorelsky, *Program for Molecular Orbital Analysis*, University of Ottawa, Ottawa, Editon edn, 2010, p. AOMix.

29 S. I. Gorelsky and A. B. P. Lever, *J. Organomet. Chem.*, 2001, **635**, 187–196.

30 *GaussView 3.0*, Gaussian Inc., Pittsburgh, PA, USA, Editon edn., 2003.

31 R. Aumann and E. O. Fischer, *Chem. Ber./Recl.*, 1968, **101**, 954–962.

32 M. Wrighton, G. S. Hammond and H. B. Gray, *J. Am. Chem. Soc.*, 1971, **93**, 4336–4337.

33 A. J. Lees, *Chem. Rev.*, 1987, **87**, 711–743.

34 M. Landman, R. Liu, R. Fraser, P. H. van Rooyen and J. Conradie, *J. Organomet. Chem.*, 2014, **752**, 171–182.

35 C. Baldoli, P. Cerea, L. Falciola, C. Giannini, E. Licandro, S. Maiorana, P. Mussini and D. Perdicchia, *J. Organomet. Chem.*, 2005, **690**, 5777–5787.

36 I. Hoskovcova, J. Rohacova, L. Meca, T. Tobrman, D. Dvorak and J. Lukvik, *Electrochim. Acta*, 2005, **50**, 4911–4915.

37 A. D. Becke, *Phys. Rev. A*, 1988, **38**, 3098–3100.

38 A. D. Becke, *J. Chem. Phys.*, 1993, **98**, 5648–5652.

39 C. T. Lee, W. T. Yang and R. G. Parr, *Phys. Rev. B: Condens. Matter*, 1988, **37**, 785–789.

40 C. T. Lee, W. T. Yang and R. G. Parr, *Theochem. J. Mol. Str.*, 1988, **40**, 305–313.

41 R. C. Morrison, W. T. Yang, R. G. Parr and C. T. Lee, *Int. J. Quantum Chem.*, 1990, **38**, 819–830.

42 W. T. Yang, R. G. Parr and C. T. Lee, *Phys. Rev. A*, 1986, **34**, 4586–4590.

43 A. Schaefer, C. Huber and R. Ahlrichs, *J. Chem. Phys.*, 1994, **100**, 5829–5835.

44 R. E. Stratmann, G. E. Scuseria and M. J. Frisch, *J. Chem. Phys.*, 1998, **109**, 8218–8224.

45 R. Bauernschmitt and R. Ahlrichs, *Chem. Phys. Lett.*, 1996, **256**, 454–464.

46 M. E. Casida, C. Jamorski, K. C. Casida and D. R. Salahub, *J. Chem. Phys.*, 1998, **108**, 4439–4449.

47 C. G. Kreiter and E. Fischer, *Angew. Chem., Int. Ed. Engl.*, 1969, **8**, 761–762.

48 A. Dreuw, B. D. Dunietz and M. Head-Gordon, *J. Am. Chem. Soc.*, 2002, **124**, 12070–12071.

49 A. Dreuw and M. Head-Gordon, *Chem. Rev.*, 2005, **105**, 4009–4037.

50 B. D. Dunietz, A. Dreuw and M. Head-Gordon, *J. Phys. Chem. B*, 2003, **107**, 5623–5629.

51 J. C. Manton, C. Long, J. G. Vos and M. T. Pryce, *Phys. Chem. Chem. Phys.*, 2014, **16**, 5229–5236.

52 J. C. Manton, S. Amirjalayer, A. Coleman, S. McMahon, E. C. Harvey, G. M. Greetham, I. P. Clark, W. J. Buma, S. Woutersen, M. T. Pryce and C. Long, *Dalton Trans.*, 2014, **43**, 17797–17805.

53 E. C. Harvey, J. Areephong, A. A. Cafolla, C. Long, W. R. Browne, B. L. Feringa and M. T. Pryce, *Organometallics*, 2014, **33**, 3309–3319.

54 E. C. Harvey, J. Areephong, A. A. Cafolla, C. Long, W. R. Browne, B. L. Feringa and M. T. Pryce, *Organometallics*, 2014, **33**, 447–456.

55 C. Long, *J. Phys. Chem. A*, 2012, **116**, 6845–6850.

56 M. W. George, C. Long, M. T. Pryce, X.-Z. Sun and K. Q. Vuong, *Organometallics*, 2012, **31**, 268–272.

57 I. P. Clark, M. W. George, G. M. Greetham, E. C. Harvey, C. Long, J. C. Manton, H. McArdle and M. T. Pryce, *J. Phys. Chem. A*, 2012, **116**, 962–969.

58 G. Picardi, T. E. Keyes, R. J. Forster and C. Long, *J. Phys. Chem. A*, 2011, **115**, 11641–11651.

59 I. P. Clark, M. W. George, G. M. Greetham, E. C. Harvey, C. Long, J. C. Manton and M. T. Pryce, *J. Phys. Chem. A*, 2011, **115**, 2985–2993.

60 E. J. Baerends and A. Rosa, *Coord. Chem. Rev.*, 1998, **177**, 97–125.

61 C. Pollak, A. Rosa and E. J. Baerends, *J. Am. Chem. Soc.*, 1997, **119**, 7324–7329.

62 A. Rosa, E. J. Baerends, S. J. A. van Gisbergen, E. van Lenthe, J. A. Groeneveld and J. G. Snijders, *J. Am. Chem. Soc.*, 1999, **121**, 10356–10365.

63 S. Villaume, A. Strich, C. Daniel, S. A. Perera and R. J. Bartlett, *Phys. Chem. Chem. Phys.*, 2007, **9**, 6115–6122.

64 C. Long, in *Photophysics of Organometallics*, ed. A. J. Lees, Springer, Berlin/Heidelberg, Editon edn, 2010, vol. 29, pp. 37–71.

65 N. Ben Arnor, S. Villaume, D. Maynau and C. Daniel, *Chem. Phys. Lett.*, 2006, **421**, 378–382.

66 The authors thank a reviewer for suggesting the use of Natural Population Analysis to calculate charges.

67 P. J. Campos, D. Sampedro and M. A. Rodriguez, *Organometallics*, 2002, **21**, 4076–4083.

